Yun et al.: Senescent cells perturb intestinal stem cell differentiation through Ptk7 induced noncanonical Wnt and YAP signaling

# Supplementary Materials

## Supplementary Figure 1

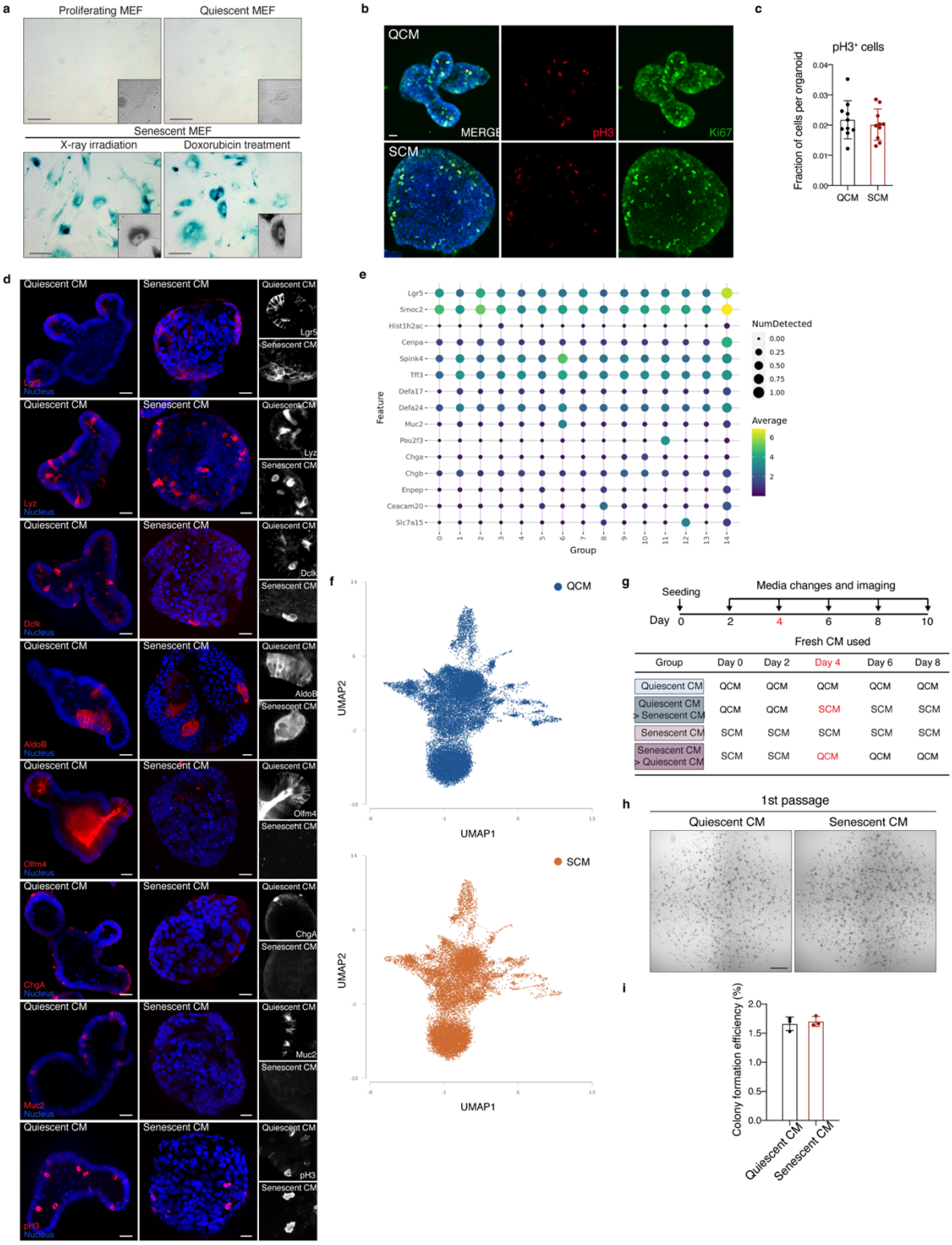

**Supplementary Figure 1 (corresponding to Fig. 1).**

(a) Representative bright field images of SA-β-gal stain in proliferating, quiescent, and senescent MEFs. Inset images show enlarged black and white images of boxed area. Scale bar: 100 μm. (b) Whole mount immunostaining of organoids for pH3 and Ki67. pH3, Ki67, and nucleus are shown in red, green, and blue respectively. Scale bar: 20 μm. (c) Fraction of phospho-Histone H3 positive cells in organoids exposed to QCM or SCM. Data are presented as the mean ± SD. n=10. (d) Whole mount immunostaining of organoids for various cell type markers. Cell type markers and nucleus are shown in red and blue respectively. Black and while enlarged images are shown at the right. Scale bar: 20 μm. n=10. (e) Identification of marker genes for each cluster, with the size of the dot corresponding to the percentage of nuclei within the nuclei expressing the gene. (f) UMAP projections showing contribution of nuclei from QCM and SCM exposed organoids. QCM was labeled in blue (top), and SCM was labeled in orange (bottom). (g) Schematic diagram showing the timeline of CM changes and imaging for each condition. (h) Representative images of the colony formation efficiency assay of organoids passaged after exposed to quiescent or senescent conditioned media and cultured in normal organoid culture media. Scale bar: 500 μm. (i) Quantification of data from (h). The percentage of cells that form organoids over a total number of seeded cells is shown (mean ± s. d.; two-tailed t-test).

## Supplementary Figure 2

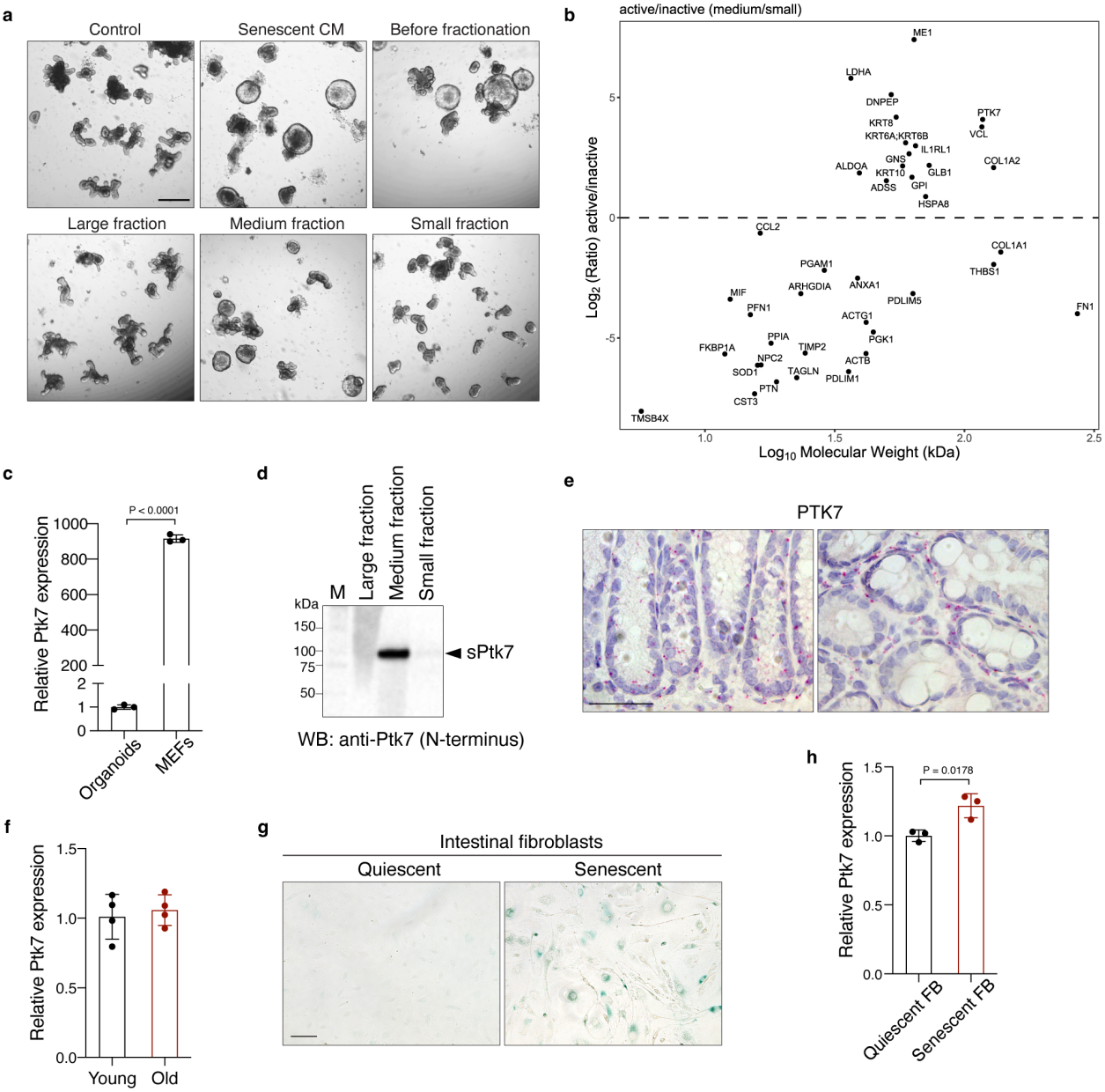


**Supplementary Figure 2 (corresponding to Fig. 2 and 3).**

(a) Representative images of organoids cultured in different fractions of senescent conditioned media collected from size exchange column. Scale bar, 200 μm. (b) Scatterplot of active:nonactive ratio (log2) versus molecular weight (log10). (c) The relative *PTK7* expression in intestinal organoids and MEFs (mean ± s. d.; n=3; two-tailed t-test). (d) Western blot for sPtk7 in different fractions of senescent conditioned media. An arrow head indicates soluble form of Ptk7; sPtk7. (e) Ptk7 transcripts in the mouse large intestine detected by RNAscope in situ hybridization. Longitudinal (left) and cross (right) sections were shown. Scale bar: 50 μm. (f) The

relative *PTK7* expression in the intestine from young and old mice (mean ± s. d.; n=4; two-tailed t-test). (g) Representative bright field images of SA-β-gal stain quiescent and senescent primary intestinal fibroblasts. Scale bar: 100 μm. (h) *PTK7* expression in quiescent and senescent intestinal fibroblasts as a ratio relative to quiescent intestinal fibroblasts. (mean ± s. d.; n=3; two-tailed t-test).

# Supplementary Figure 3

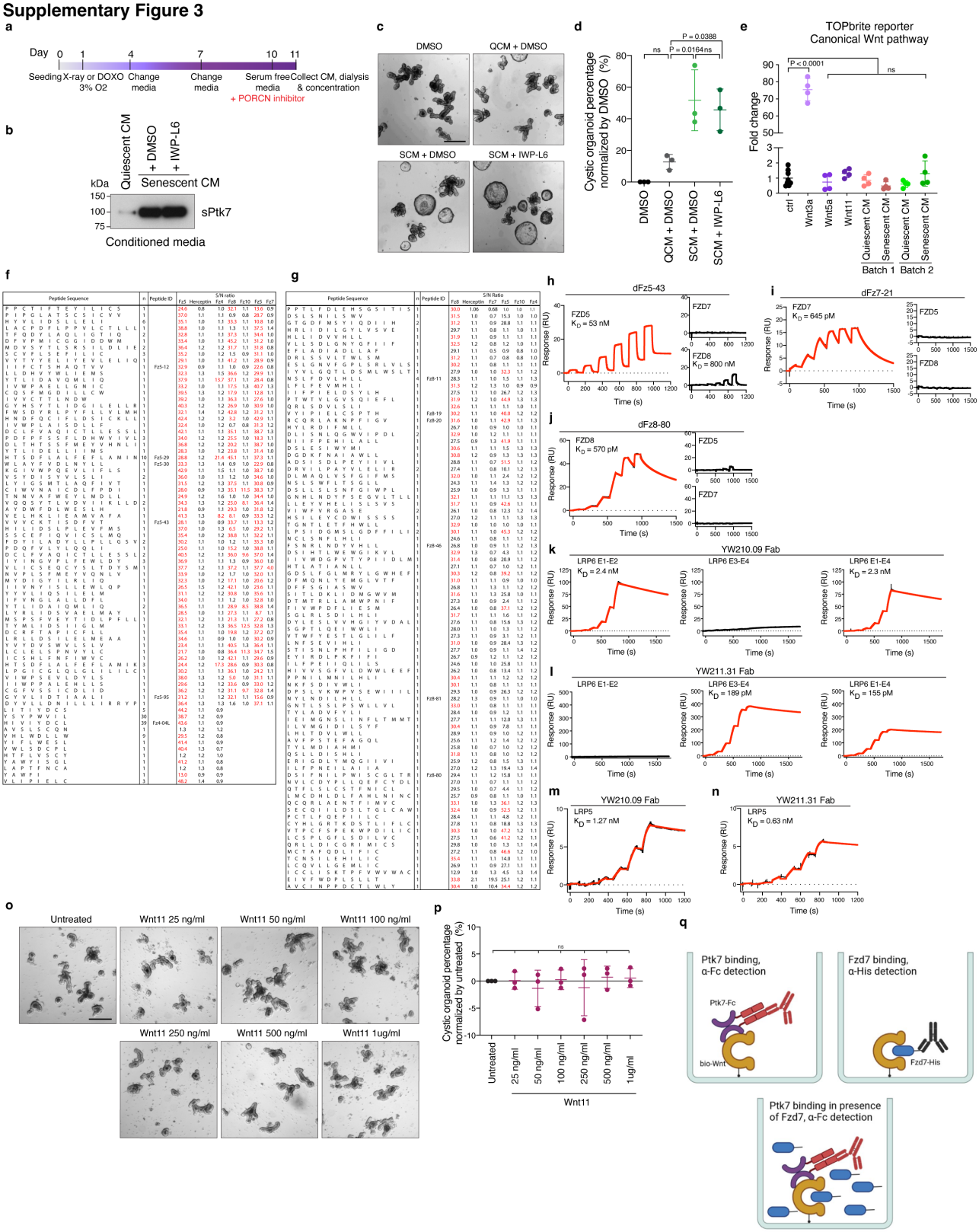

**Supplementary Figure 3 (corresponding to Fig. 4).**

(a) Schematic diagram showing induction of cellular senescence in fibroblasts, PORCN inhibitor treatment, and conditioned media collection. (b) Western blot for sPtk7 in CM collected from quiescent and senescent MEFs treated with vehicle or PORCN inhibitor for 24 hrs. Conditioned media corresponding to the same number of cells was loaded. (c) Representative images of organoids cultured in corresponding CM. Scale bar, 200 μm. (d) Quantification of data from (c) shows no change in the percentage of cystic organoids by inhibition of Wnt secretion. Data are presented as means ± s. d. One-way ANOVA followed by Tukey's post-hoc multiple comparison tests. Each dot represents a result from organoids established from a mouse, n=3. (e) TOPbrite dual-luciferase Wnt reporter assay. The graph shows fold changes in luminescence for the indicated treatments normalized to control. Data are presented as means ± s. d. One-way ANOVA followed by Tukey's post-hoc multiple comparison tests. n=4.

(f) Sequences and binding of phage display derived peptides selected against hFZD5-CRD. Peptide sequences are given in single letter amino acid code. n reflects how often the peptide sequence was found in the analyzed phage pool. Peptide ID shows the name of peptides that were synthesized and further analyzed. S/N ratio gives the ratio of phage ELISA signal with immobilized FZD-CRDs or Herceptin over signal with no immobilized protein (BSA blocking only).

**(g)** Sequences and binding of phage display derived peptides selected against hFZD8-CRD. Peptide sequences are given in single letter amino acid code. n reflects how often the peptide sequence was found in the analyzed phage pool. Peptide ID shows the name of peptides that were synthesized and further analyzed. S/N ratio gives the ratio of phage ELISA signal with immobilized FZD-CRDs or Herceptin over signal with no immobilized protein (BSA blocking only).

(h-j) Surface plasmon resonance (SPR) of dFz5-43, dFz7-21, and dFz8-80. (h) Binding of peptide dFz5-43 to different human FZD-CDRs probed by surface plasmon resonance. Binding response is shown in black. For FZD5-CDR, the fit to a 1:1 kinetic model is shown in red. Equilibrium fitting with resulting KDs is shown. (i) Binding of peptide dFz7-21 to different human FZD-CDRs probed by surface plasmon resonance. Binding response is shown in black. For FZD7-CDR, the fit to a 1:1 kinetic model is shown in red. Equilibrium fitting with resulting KDs is shown. (j) Binding of peptide dFz8-80 to different human FZD-CDRs probed by surface plasmon resonance. Binding response is shown in black. For FZD8-CDR, the fit to a 1:1 kinetic model is shown in red. Equilibrium fitting with resulting KDs is shown. (k-n) Surface plasmon resonance (SPR) of YW210.09 and YW211.31.62. Binding of Fabs YW210.09 and YW211.31.62 to the extracellular domain of LRP6 (k, l) and to the extracellular domain of LRP5 (m, n). Binding responses are shown in black overlaid with fit to a 1:1 kinetic model in red. (o) Representative images of

organoids treated with different concentrations of recombinant Wnt11. Scale bar, 200 μm. (p) Quantification of data from (o) shows no effect on intestinal organoid morphology by Wnt11. Data are presented as means ± s. d. One-way ANOVA followed by Tukey's post-hoc multiple comparison tests. Each dot represents a result from organoids established from a mouse, n=3. (q) Schematic diagram illustrating interaction of Ptk7, Wnt ligands, and Fzd7. The figure was created with BioRender.com.

## Supplementary Figure 4

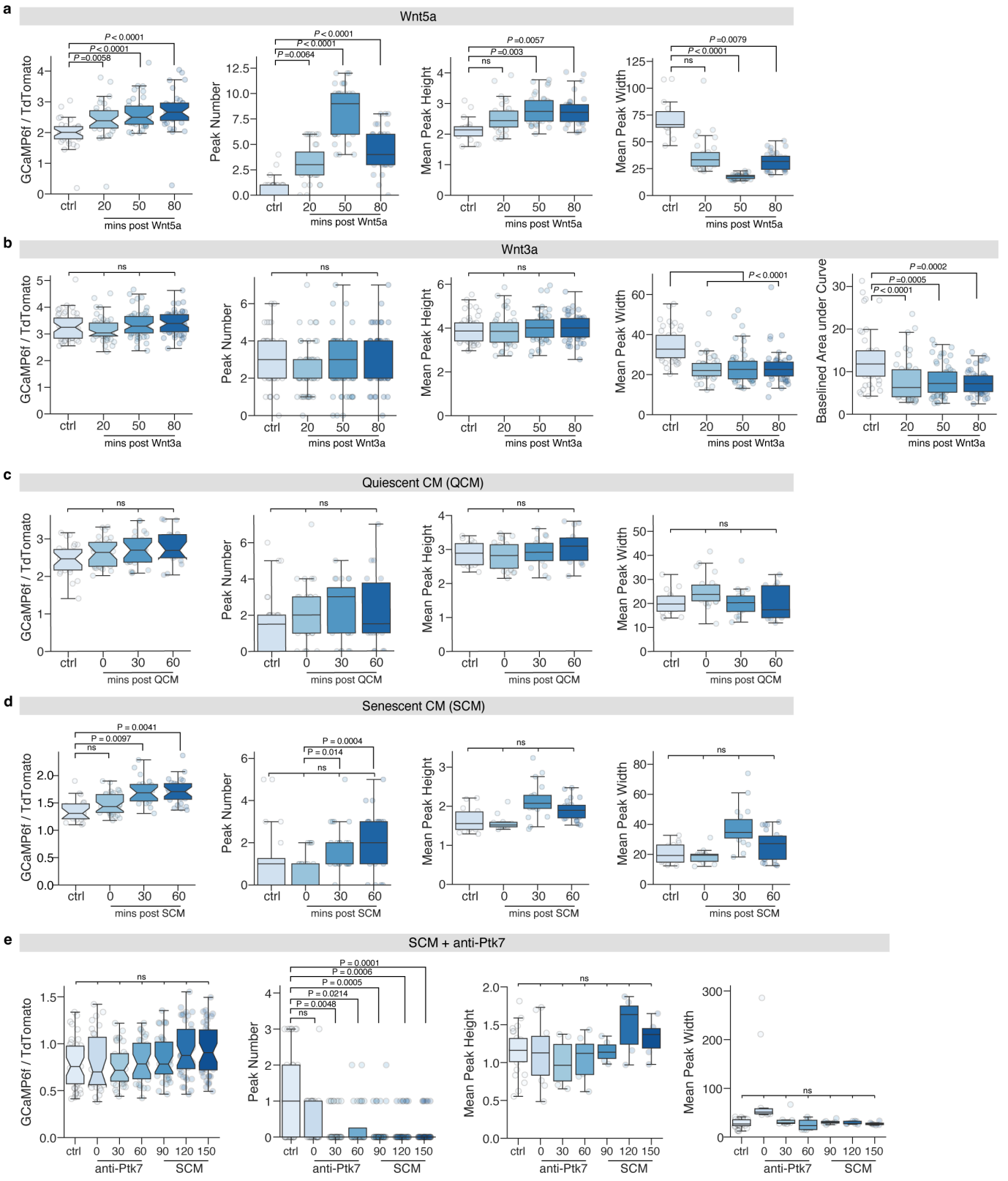

**Supplementary Figure 4 (corresponding to Fig. 5).**

(a-e) Boxplots showing GCaMP6f/TdTomato intensity ratio, $Ca^{2+}$ peak number, mean $Ca^{2+}$ peak height, and mean $Ca^{2+}$ peak width of each time points from live imaging before and after addition of Wnt5a (a), Wnt3a (b), quiescent CM (c), senescent CM (d), and anti-Ptk7 antibodies followed by senescent CM (e). Boxplots display median ± interquartile range with whiskers marking 1.5 times the interquartile range. The graph shows results from a representative experiment. Kruskal-Wallis test followed by Dunn's post-hoc multiple comparison tests. n=5, 5, 3, 6, and 6 in (a), (b), (c), (d), and (e) respectively.

# Supplementary Figure 5

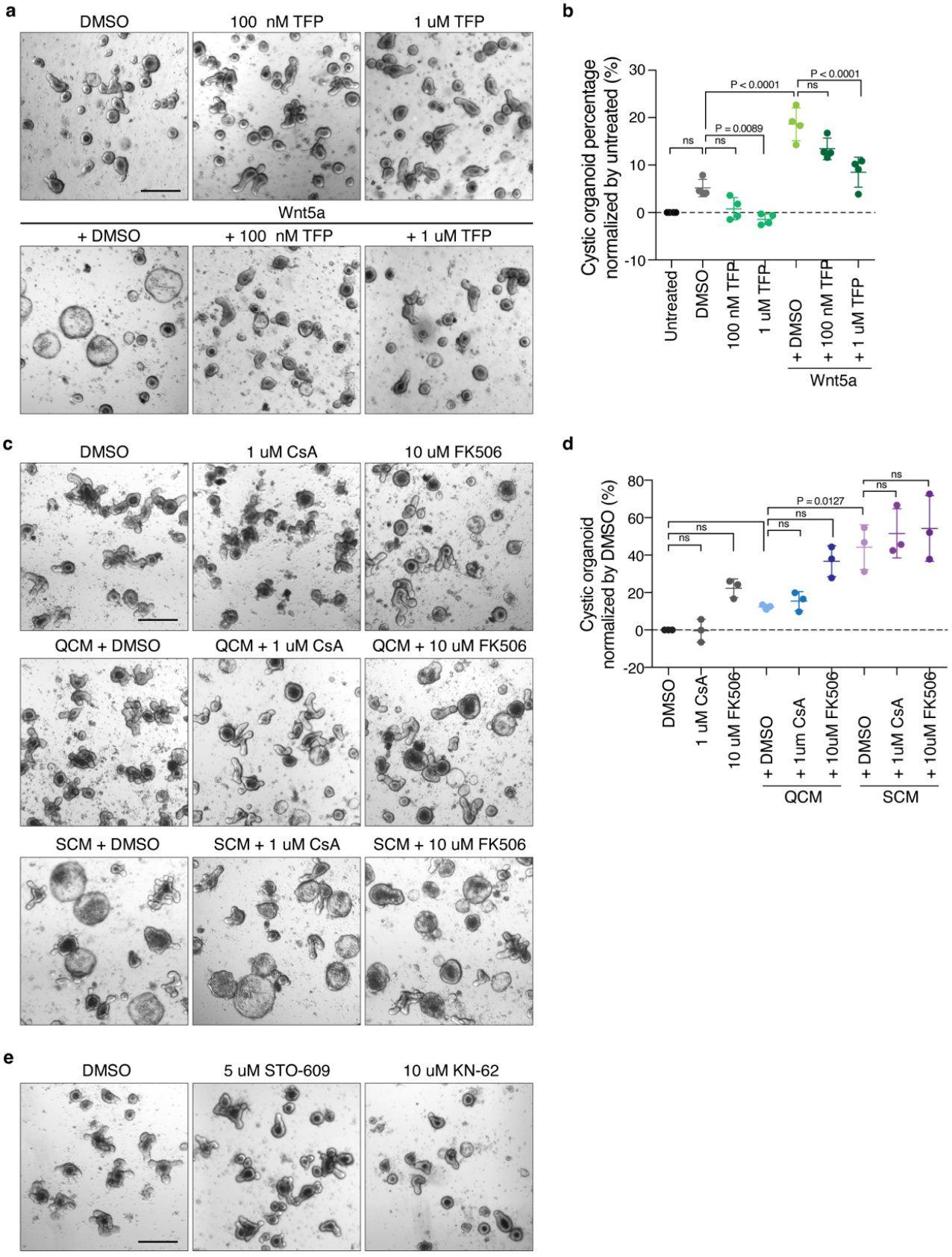

**Supplementary Figure 5 (corresponding to Fig. 5).**

(a) Representative images of organoids cultured in Wnt5a with DMSO, 100 nM TFP, or 1 μM TFP. Scale bar: 200 μm. (b) Quantification of data from (a). (c) Representative images of organoids cultured in QCM or SCM with DMSO, 1 μM CsA, or 10 μM FK506. Scale bar: 200 μm. (d) Quantification of data from (c). In (b) and (d), data are presented as means ± s. d. percentage of cystic organoids. Each dot represents a result from organoids established from a mouse, n=4 and 3 in (b) and (d) respectively. One-way ANOVA followed by Tukey's post-hoc multiple comparison tests. (e) Representative images of organoids treated with DMSO, 5 μM STO-609, or 10 μM KN-62. Scale bar: 200 μm

# Supplementary Figure 6

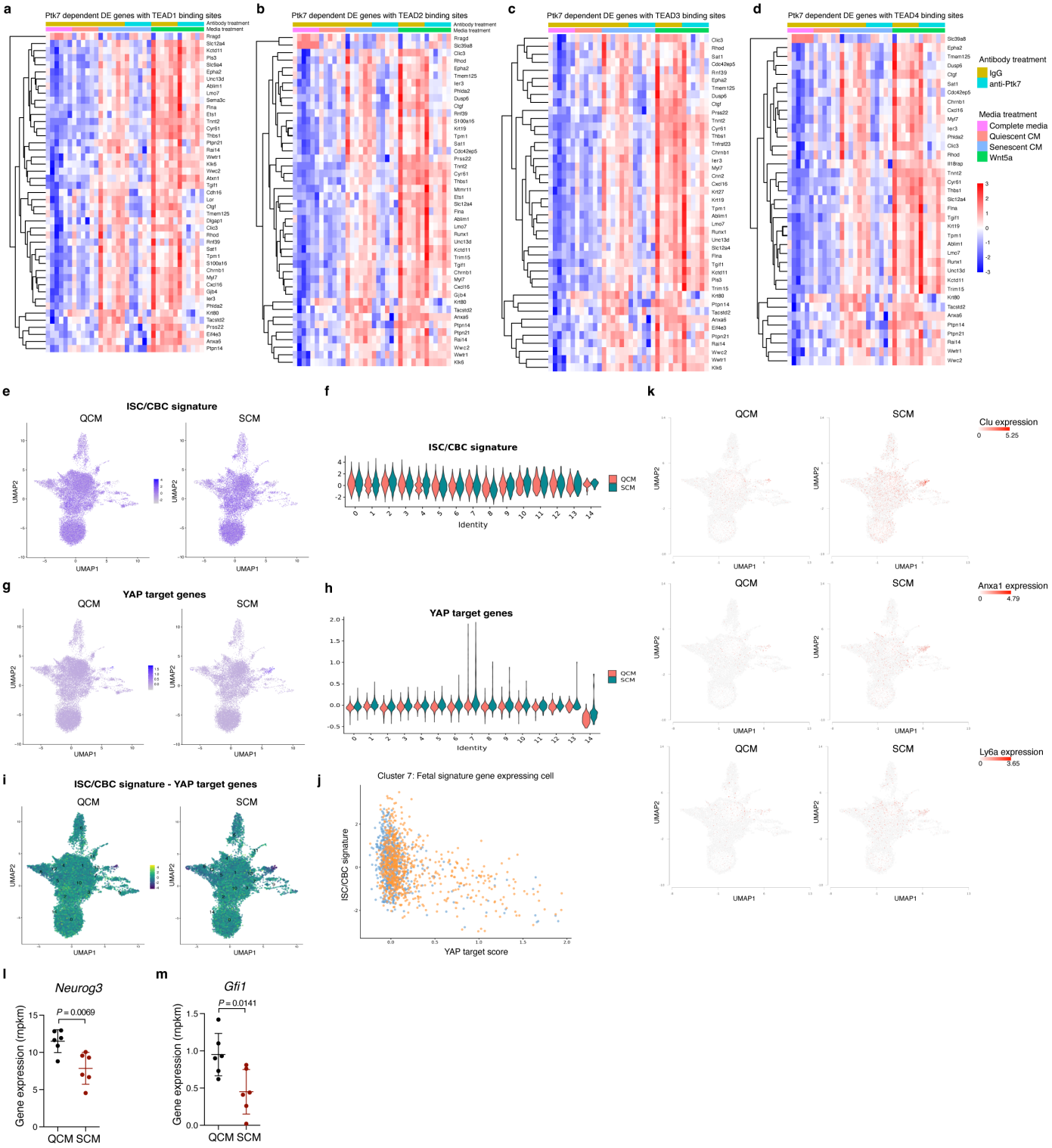

**Supplementary Figure 6 (corresponding to Fig. 6).**

(a-d) Heatmaps showing expression of Ptk7 dependent DE genes with different TEAD binding motifs- TEAD1 (a), TEAD2 (b), TEAD3 (c), and TEAD4 (d). (e-h) UMAPs and violin plots for the relative mean expression levels of ISC/CBC signature genes (e, f) and YAP target genes (g, h). P-values for each cluster in (h) - cluster 0 is p= 0.00046, clusters 2, 5, 6, 7, 8, 9, 14 are $p<0.0001$, cluster 3 is p=0.005, and cluster 10 is p=0.038. Two-tailed t-test. (i) Difference in ISC/CBC signature and YAP target genes on the UMAPs. (j) Cluster 7 fetal signature gene expressing cells plotted for ISC/CBC signature and YAP target score. (k) Expression of fetal signature genes; Clu (top), Anxa1 (middle), and Ly6a (bottom) on the UMAP. (l, m) *Neurog3* and *Gfi1* expression in organoids exposed to QCM and SCM. mean $\pm$ s. d.; n=6; two-tailed t-test.

## Supplementary Figure 7

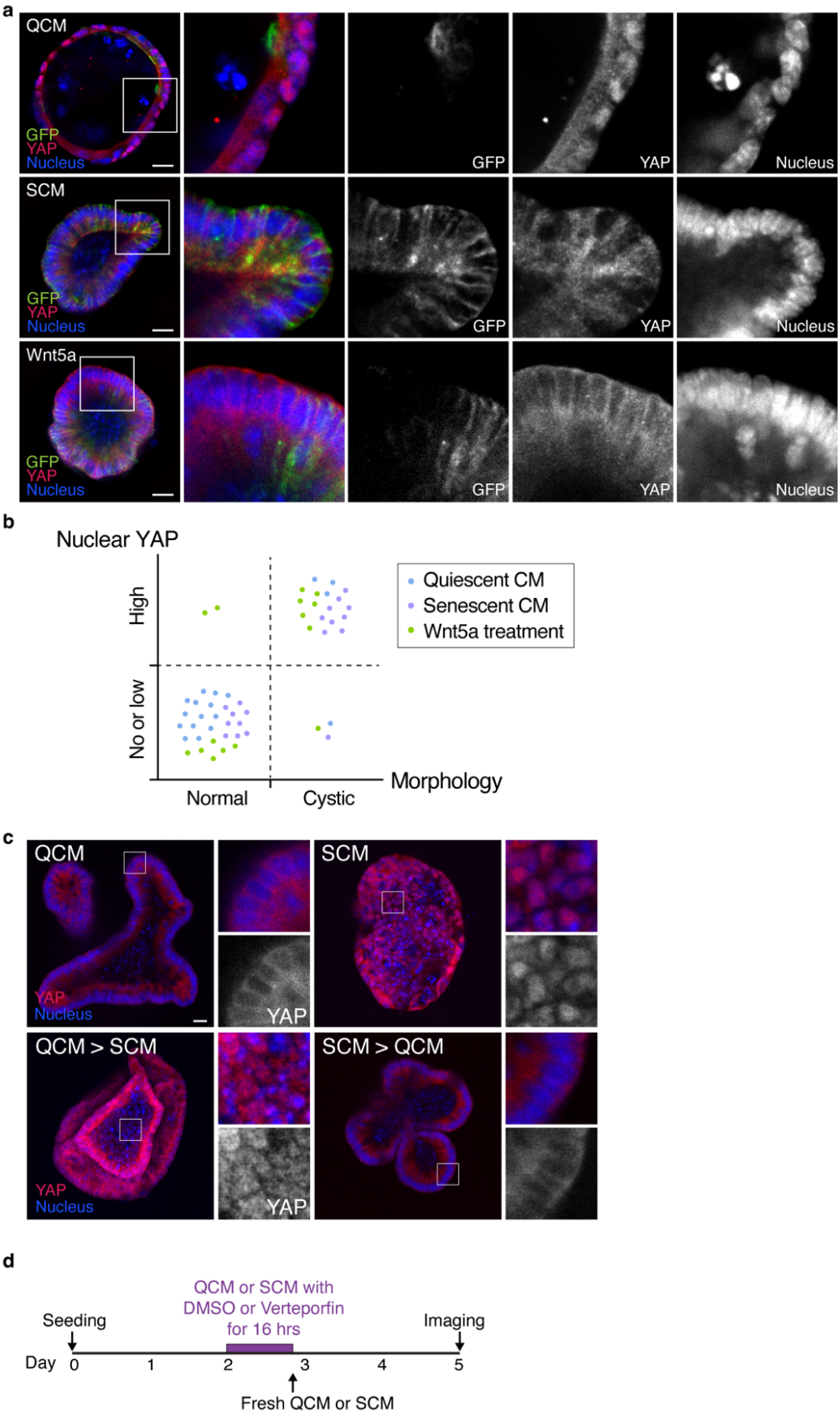

**Supplementary Figure 7 (corresponding to Fig. 7).**

(a) Whole mount immunostaining of organoids for YAP. Organoids established from Lgr5-DTR-GFP mice were stained for GFP, YAP, and nucleus (DAPI) in green, red, and blue respectively. Nuclear localization of YAP is observed in cystic organoids grown in quiescent conditioned media. Enlarged images of boxed area are shown at the right. Scale bar: 20 μm. (b) Correlation between nuclear YAP levels and organoid morphology. Each dot represents an organoid from QCM, SCM, and Wnt5a labeled in blue, purple, and green respectively. (c) Whole mount immunostaining of organoids for YAP. YAP and nucleus are shown in red and blue respectively. Representative images of an organoid from each condition are shown. n=4 per each condition. Enlarged images of boxed area are shown at the right. Scale bar: 20 μm. (d) Schematic diagram showing changes of CM and addition of DMSO or Verteporfin.

**Supplementary Table 1: List of TaqMan assay probes used for qPCR**

| Target | Company | Cat. No. |
|---|---|---|
| *GAPDH* | Thermo Fisher Scientific | Mm99999915_g1 |
| *PTK7* | Thermo Fisher Scientific | Mm00613367_g1 |
| *LGR5* | Thermo Fisher Scientific | Mm00438890_m1 |
| *OLFM4* | Thermo Fisher Scientific | Mm01320260_m1 |
| *Lyz1* | Thermo Fisher Scientific | Mm00657323_m1 |
| *CHGA* | Thermo Fisher Scientific | Mm00514341_m1 |
| *MUC2* | Thermo Fisher Scientific | Mm00458299_m1 |
| *ALPI* | Thermo Fisher Scientific | Mm01285814_g1 |
| *MKI67* | Thermo Fisher Scientific | Mm01278617_m1 |

**Supplementary Table 2: Antibodies used in this study**

| Antibody | Company | Cat. No. | Dilution |
|---|---|---|---|
| anti-Ki67 | BD Biosciences | 550609 | 1:100 |
| anti-phospho-Histone H3 | EMD Millipore | 06-570 | 1:250 |
| anti-GFP | Abcam | ab13970 | 1:400 |
| anti-Olfm4 | Cell Signaling Technology | 39141S | 1:200 |
| anti-Lyz | Dako | EC 3.2.1.17 | 1:200 |
| anti-ChgA | Novus Biologicals Biologicals | NB120-15160 | 1:200 |
| anti-Dclk | Abcam | ab31704 | 1:100 |
| anti-Muc2 | Abcam | ab134119 | 1:100 |
| anti-Aldolase B | Abcam | ab75751 | 1:100 |
| Anti-Lrp5/6 Fabs | - | - | 10 μg/ml |
| Rabbit IgG | Thermo Fisher Scientific | 02-6102 | 5 μg/ml |
| anti-Ptk7 | Sigma-Aldrich | HPA003222 | 5 μg/ml or 1:500 |
| anti-YAP | Cell Signaling Technology | 14074S | 1:200 |
| anti-MMP14 | Abcam | ab51074 | 1:2000 |
| anti-alpha-Tubulin | Cell Signaling Technology | 3873S | 1:5000 |
| anti-beta-Actin | Cell Signaling Technology | 8457S | 1:10000 |
| anti-Vimentin | Sigma-Aldrich | AB5733 | 1:200 |
| anti-hIgG1-Fc-HRP | Thermo Fisher Scientific | A-10648 | 1:5000 |
| anti-His-tag-HRP | Abcam | ab1187 | 1:5000 |
| anti-rabbit IgG-HRP | GE Healthcare | NA934 | 1:5000 |
| anti-chicken IgY Alexa Fluor 488 | Jackson ImmunoResearch Laboratories | 703-545-155 | 1:500 |
| Anti-rabbit IgG Alexa Fluor Plus 555 | Thermo Fisher Scientific | A32794 | 1:500 |

**Supplementary Table 3: Recombinant proteins used in this study**

| Recombinant protein | Company | Cat. No. |
|---|---|---|
| hmWnt5a | R&D Systems | 645-WN-010 |
| Biotinylated hmWnt5a | R&D Systems | BT645 |
| mWnt3a | R&D Systems | 1324-WN-010 |
| Biotinylated mWnt3a | R&D Systems | BT1324 |
| hWnt11 | R&D Systems | 6179-WN-010 |
| Ptk7 | R&D Systems | 9799-TK |
| FZD5 | R&D Systems | 5988-FZ |
| FZD7 | R&D Systems | 6178-FZ |
| FZD8 | R&D Systems | 6129-FZ |
| LRP5 | R&D Systems | 7344-LR |

**Supplementary Table 4: Compounds and inhibitors used in this study**

| Compound | Company | Cat. No. | Concentration |
|---|---|---|---|
| Doxorubicin | Sigma-Aldrich | 44583 | 250 nM |
| DMSO | Sigma-Aldrich | D2650 | - |
| TAPI-1 | Sigma-Aldrich | 579053 | 50 uM |
| GM6001 | Sigma-Aldrich | 364206 | 20 uM |
| IWP-L6 | Sigma-Aldrich | 5048190001 | 40 nM |
| Trifluoperazine | Sigma-Aldrich | T8516 | 1 uM |
| STO-609 | Selleck Chemicals | S8274 | 5 uM |
| KN-62 | Selleck Chemicals | S7422 | 10 uM |
| Cyclosporin A | Selleck Chemicals | S2286 | 1 uM |
| FK506 | Selleck Chemicals | S5003 | 10 uM |
| Verteporfin | Sigma-Aldrich | SML0534 | 250 nM, 500 nM |
| TED347 | Selleck Chemicals | S8951 | 2 uM |
| dFz5-43 | - | - | 80 uM |
| dFz7-21 | - | - | 50 uM |
| dFz8-80 | - | - | 80 uM |